

Figure S1

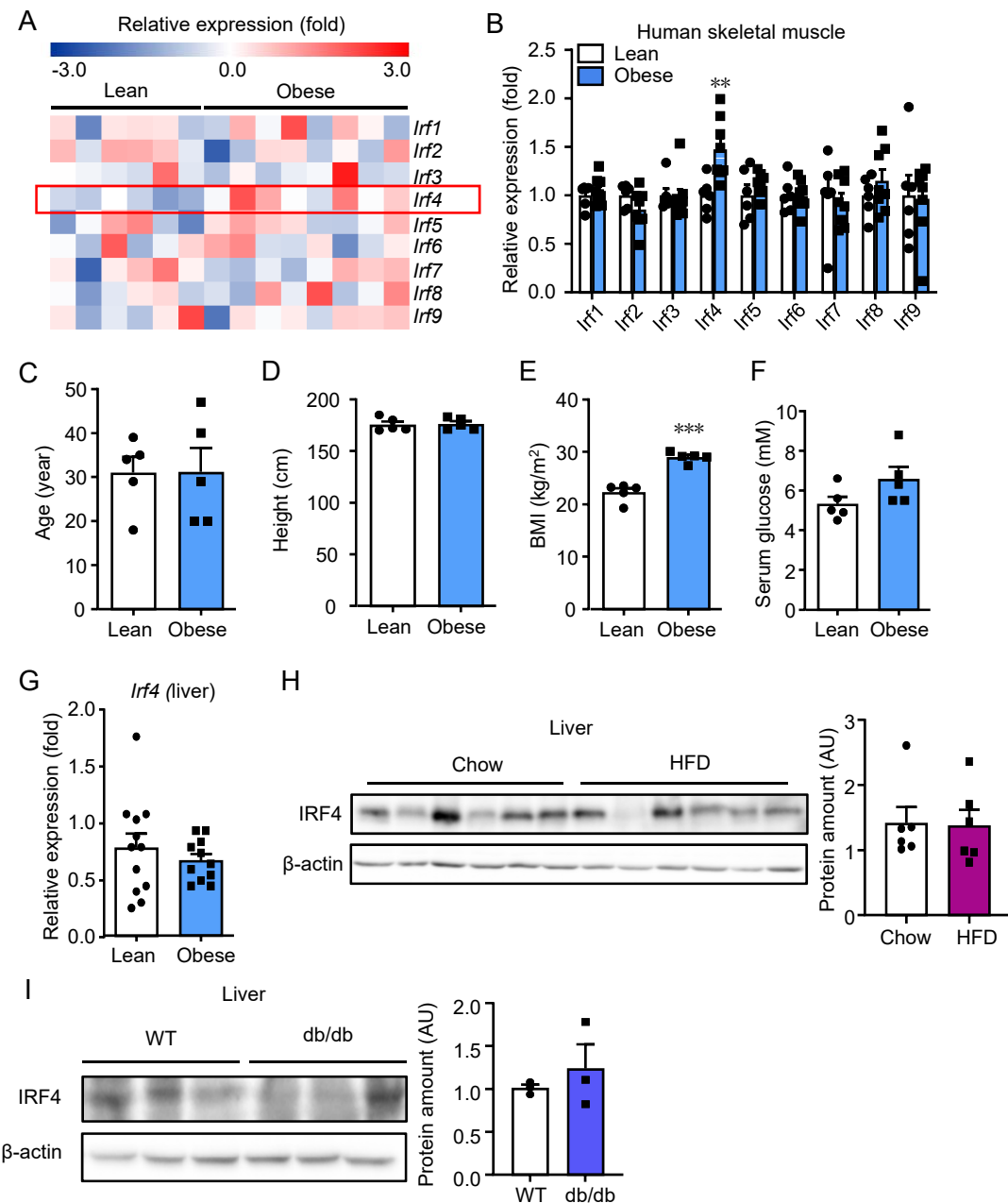


Figure S1. Association between IRF4 and obesity. **A** and **B**, The expression of IRFs in microarray experiments using human skeletal muscle tissues from obese and lean subjects. The data were extracted from GEO GSE474 ($n=6-8$, $**p<0.01$). **C-F**, The age, height, BMI and serum glucose of subjects with lean or obesity ($n=5$, $***p<0.001$). **G**, The expression of *Irf4* using human liver data from GEO GSE 126848 ($n=11-12$). **H**, Western blot analysis of the expression of IRF4 in Liver of mice on HFD or chow diet. Protein amount was quantified using Image J ($n=6$). **I**, Western blot analysis of the expression of IRF4 in Liver of db/db mice and WT mice. Protein amount was quantified using Image J ($n=3$). All results are expressed as means \pm SEM. BMI, body mass index.

Figure S2

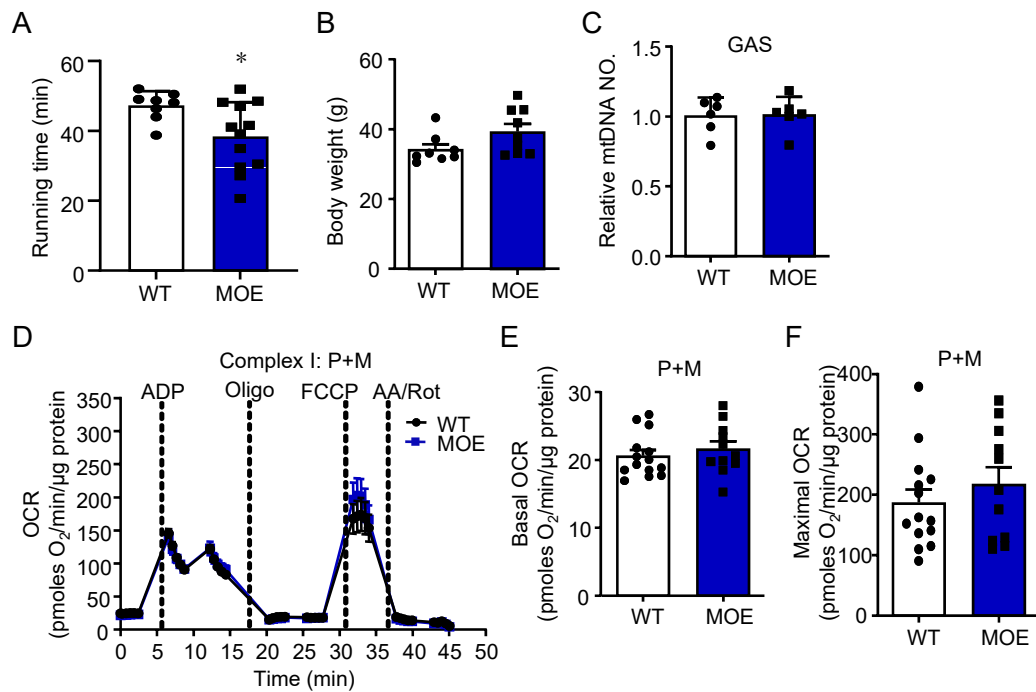


Figure S2. Overexpression of IRF4 in skeletal muscle promotes DIO. **A**, The running time of male MOE and WT mice (n=7-12, *p<0.05). **B**, The body weight of male MOE and WT mice on 8-week HFD (n=8). **C**, The relative mitochondria DNA copy number of GAS in MOE and WT mice (n=6). **D**, Seahorse assays of OCR in the isolated mitochondria from GAS of MOE and WT mice (n=11-14). **E** and **F**, The basal and maximal OCR of mitochondria from GAS in MOE and WT mice (n=11-14). All results are expressed as means ± SEM. P, pyruvate; M, malate; GAS, gastrocnemius.

Figure S3

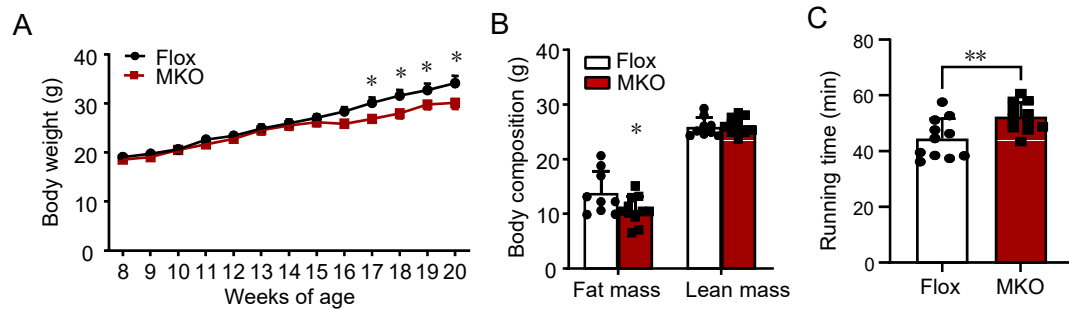


Figure S3. Ablation of IRF4 in skeletal muscle attenuates DIO. **A**, The body weight of female MKO and Flox mice on HFD (n=8-10, *p<0.05). **B**, The body composition of female MKO and Flox mice on 12-week HFD (n=8-10, *p<0.05). **C**, The running time of male MKO and Flox mice (n=10-11, *p<0.05). All results are expressed as means ± SEM.

Figure S4

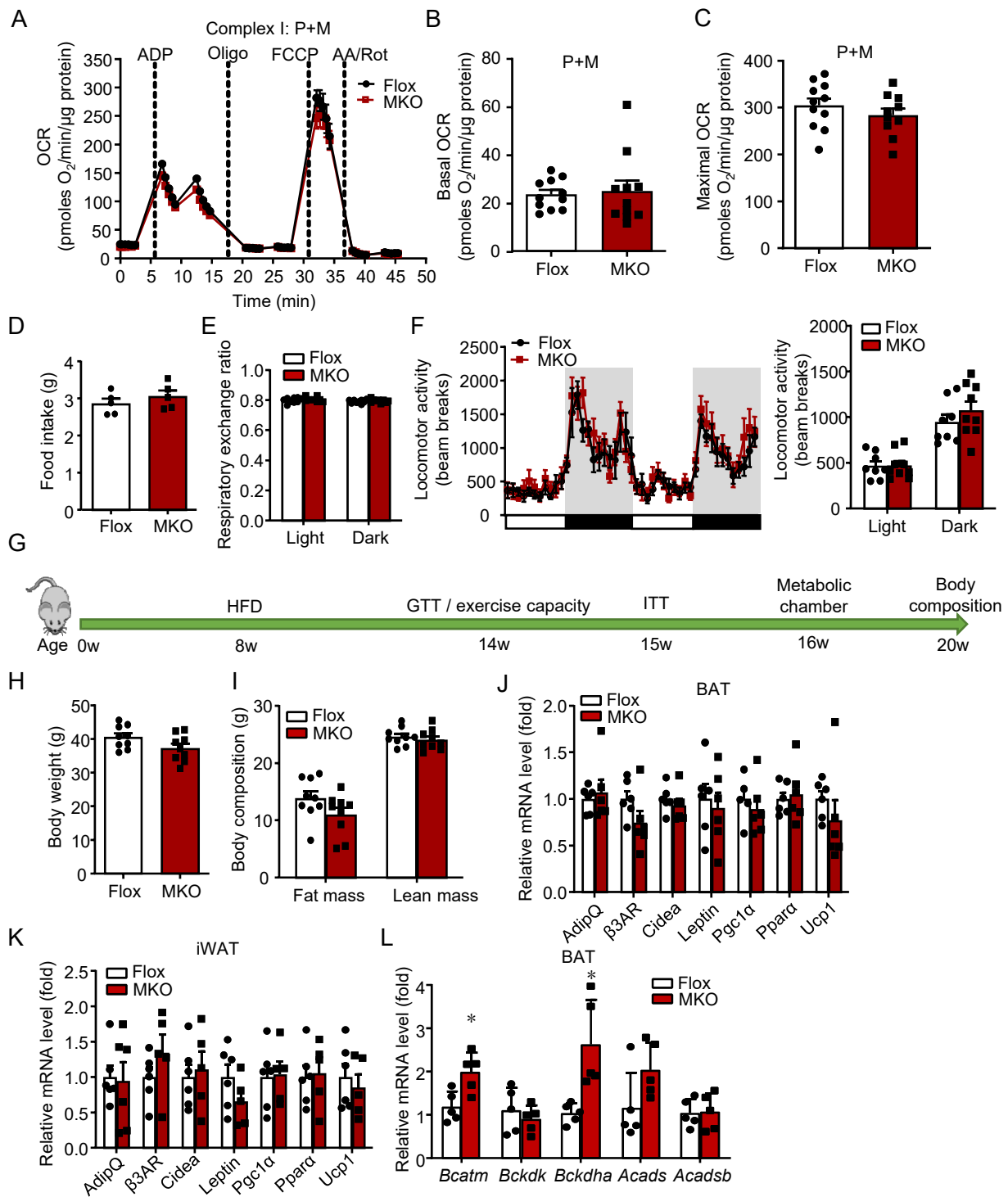


Figure S4. IRF4 in skeletal muscle has no effects on food intake, RER or locomotor activity. **A**, Seahorse assays of complex I OCR in the isolated mitochondria from GAS of MKO and Flox mice ($n=11$). **B** and **C**, The basal and maximal OCR of mitochondrial complex I from GAS in MKO and Flox mice ($n=11$). **D**, Food intake of male MKO and Flox mice on 12-week HFD ($n=5$). **E**, Respiratory exchange ratio of male MKO and Flox mice on 8-week HFD ($n=9$). **F**, The locomotor activity of male MKO mice and Flox mice on 8-week HFD ($n=9$). **G**, The timeline of mice experiment. **H**, The body weight of male MKO and Flox mice on 8-week HFD ($n=9$). **I**, The body composition of male MKO and Flox mice on 8-week HFD ($n=9-10$). **J** and **K**, The mRNA expression of thermogenic genes in BAT and iWAT of male MKO and Flox mice ($n=6$). **L**, The mRNA expression of BCAAs catabolic genes in BAT of MKO and Flox mice ($n=5$, $*p<0.05$). All results are expressed as means \pm SEM. P, pyruvate; M, malate; GAS, gastrocnemius; HFD, high fat diet; BAT, brown adipose tissue; iWAT, inguinal white adipose tissue.

Figure S5

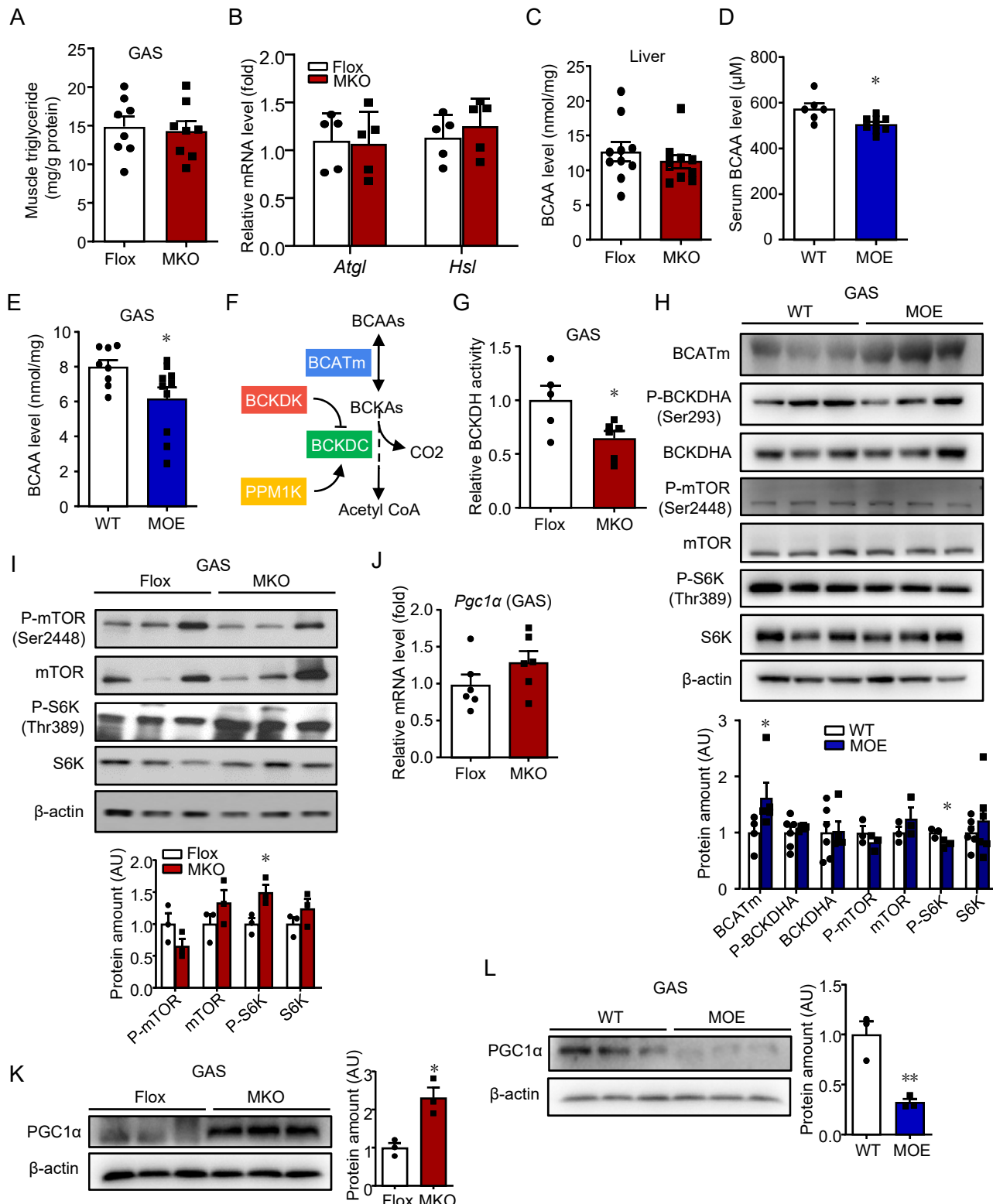


Figure S5. IRF4 regulates macronutrients metabolism and mTOR pathway in skeletal muscle. **A**, GAS TG level (n=8). **B**, qPCR analysis of lipolytic genes expression (n=5). **C**, The BCAA level in liver of MKO and Flox mice (n=10). **D** and **E**, Serum and GAS BCAA level of MOE and WT mice (n=6-10, *p<0.05). **F**, BCAAs metabolism pathway in skeletal muscle. **G**, The relative BCKDH activity in GAS of male MKO and Flox mice on HFD (n=5-6, *p<0.05). **H**, Western blot analysis of BCAA catabolism and mTOR signaling pathway in GAS from MOE and WT mice on HFD (n=3, *p< 0.05). **I**, Western blot analysis of mTOR signaling pathway in GAS from MKO and Flox mice on HFD. Protein amount was quantified using Image J (n=3, *p< 0.05). **J**, The mRNA expression of Pgc1 α in GAS of MKO and Flox mice (n=6). **K**, Western blot analysis of the expression of PGC1 α in GAS of MKO and Flox mice. Protein amount was quantified using Image J (n = 3, *p< 0.05). **L**, Western blot analysis of the expression of PGC1 α in GAS of MOE and WT mice (n=3, **p< 0.01). All results are expressed as means \pm SEM. GAS, gastrocnemius.

Figure S6

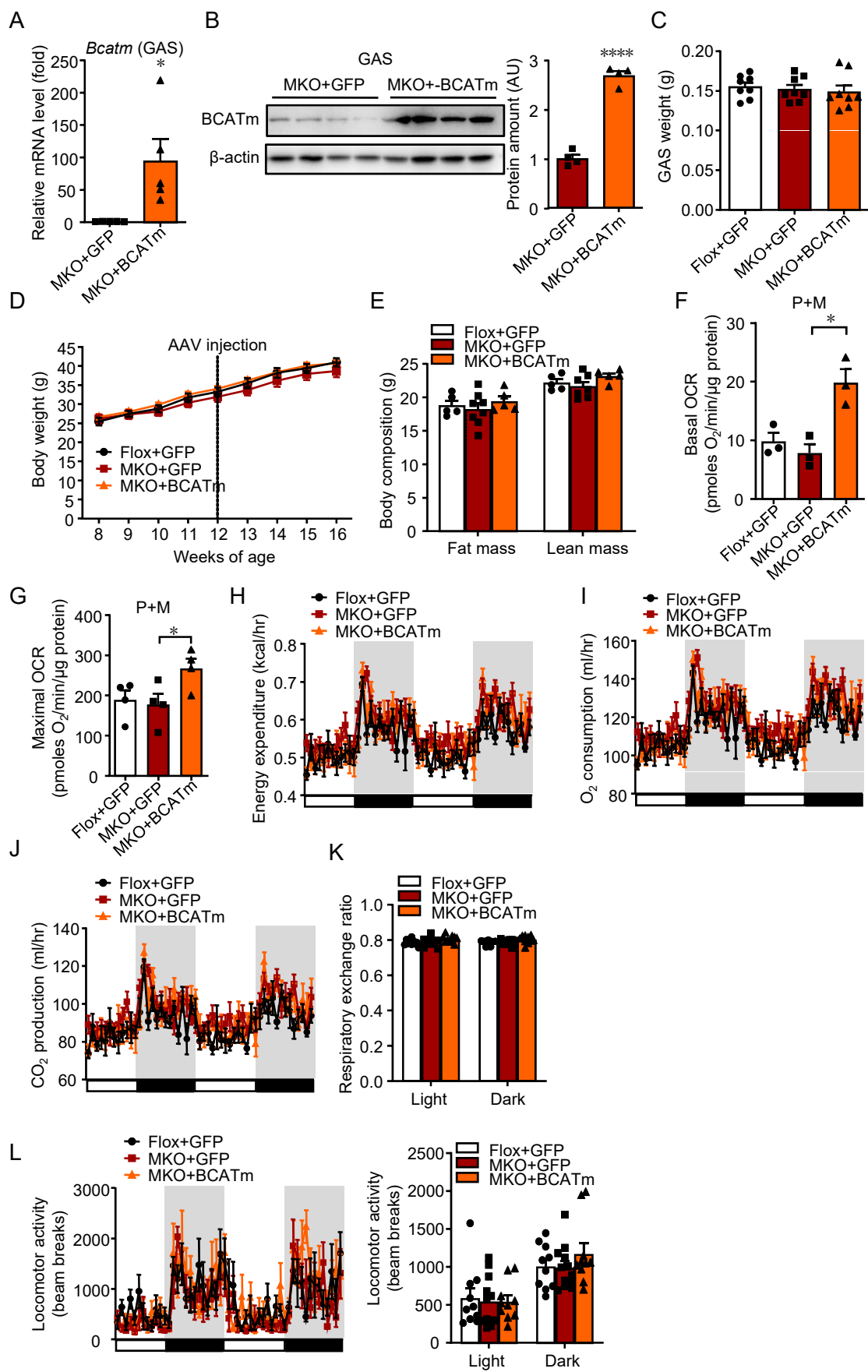


Figure S6. BCATm contributes to IRF4-induced metabolic phenotype. **A**, qPCR analysis of *Bcatm* in GAS of MKO+AAV-BCATm mice, MKO+AAV-GFP mice, and Flox+AAV-GFP mice (n=5, *p<0.05). **B**, Western blot analysis of the expression of BCATm in GAS of MKO+AAV-BCATm mice and MKO+AAV-GFP mice. Protein amount was quantified using Image J (n=4, ****p<0.0001). **C**, The weight of GAS in MKO+AAV-BCATm mice, MKO+AAV-GFP mice, and Flox+AAV-GFP mice on HFD on 8-week HFD (n=8). **D**, The body weight of MKO+AAV-BCATm mice, MKO+AAV-GFP mice, and Flox+AAV-GFP mice on HFD (n=8). **E**, The body composition of MKO+AAV-BCATm mice, MKO+AAV-GFP mice, and Flox+AAV-GFP mice on HFD (n=5-8). **F** and **G**, The basal and maximal OCR of mitochondrial complex I from GAS in AAV injected mice (n=3). **H-J**, The energy expenditure, oxygen consumption, and carbon dioxide production of male MKO+AAV-BCATm mice, MKO+AAV-GFP mice, and Flox+AAV-GFP mice on 8-week HFD (n=10-12, body weight matched). **K**, Respiratory exchange ratio of MKO+AAV-BCATm mice, MKO+AAV-GFP mice, and Flox+AAV-GFP mice on 8-week HFD (n=10-12). **L**, The locomotor activity of MKO+AAV-BCATm mice, MKO+AAV-GFP mice, and Flox+AAV-GFP mice on 8-week HFD (n=10-12). All results are expressed as means ± SEM. GAS, gastrocnemius.

Figure S7

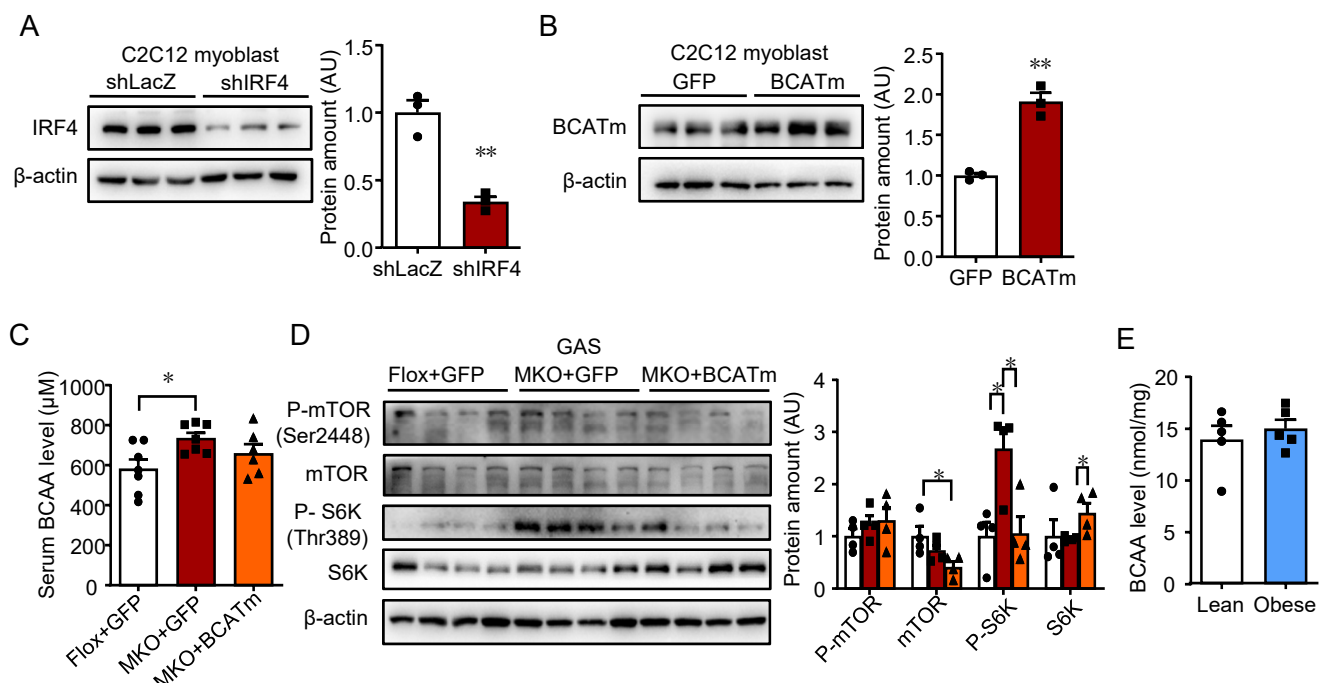


Figure S7. BCATm accounts for changed BCAAs metabolism and mTOR pathway in IRF4-deleted skeletal muscle. **A** and **B**, Western blot analysis of the expression of IRF4 and BCATm in C₂C₁₂ myoblast. Protein amount was quantified using Image J (n=3, **p<0.01). **C**, Serum BCAA level of male MKO+AAV-BCATm mice, MKO+AAV-GFP mice, and Flox+AAV-GFP mice (n=6-7, *p<0.05). **D**, Western blot analysis of mTOR signaling pathway in GAS of MKO+AAV-BCATm mice, MKO+AAV-GFP mice, and Flox+AAV-GFP mice. Protein amount was quantified using Image J (n = 4, *p<0.05). **E**, The BCAA level in skeletal muscle of lean and obese subjects (n=5). All results are expressed as means ± SEM.